Modeling Droplet Collision and Coalescence in an Icing Wind Tunnel and the Influence of these Processes on Droplet Size Distribution

László E. Kollár, Masoud Farzaneh, Anatolij R. Karev

NSERC/Hydro-Québec/UQAC Industrial Chair on Atmospheric Icing of Power Network Equipment (CIGELE) and Canada Research Chair on Atmospheric Icing Engineering of Power Network (INGIVRE) at University of Québec at Chicoutimi, 555 Boulevard de l'Université, Chicoutimi, Québec G7H 2B1, Canada (http://www.cigele.ca)

Abstract

A theoretical model of a two-phase air/dispersed water spray flow in an icing wind tunnel is presented here. The mutual interactions taking place within the dispersed phase known as binary droplet collisions, as well as gravitational sedimentation are considered. Where large droplets and low air stream velocities are concerned, the effect of gravity on droplet dynamics is considerable. Gravity causes the vertical deflection of droplet trajectories and an increase in liquid water content (LWC) in the bottom half of the wind tunnel. Droplet collision tends to influence the size, trajectory and velocity of droplets thus affecting the characteristics of the flow and, thereby, the formation of ice on the object placed in the wind tunnel. The present model simulates droplet motion and droplet collision in an icing wind tunnel, where it may be observed that bouncing, stable coalescence, or coalescence followed by separation are the possible outcomes of collision. In the theoretical examination, firstly, the effect of gravity on the vertical deflection of droplet trajectories and on

the vertical distribution of the LWC near the icing object are taken into account, while droplet collision is disregarded. Then both factors are considered and collision outcome is determined together with the size and velocity of post-collision droplets. The initial droplet size distribution (DSD), as it occurs at the nozzle outlet, is estimated by a curve in accordance with previous experimental results. The DSD is determined theoretically near the icing object, which makes it possible to calculate the median volume diameter and the LWC of the aerosol cloud. The simulation results with regard to the LWC are compared to the experimental results obtained in this research and a satisfactory qualitative coincidence is to be found between them.

Key words: Droplet collision and coalescence, Droplet size distribution, Liquid water content

---

1 Introduction

The droplet size distribution (DSD) of an aerosol cloud together with its temperature, the free stream velocity and the liquid water content (LWC) are among the most important factors affecting atmospheric icing processes. The DSD influences the trajectories of the dispersed phase particles which collide with the icing object. Several models have been developed to study ice accretion and to examine how both droplet size and trajectory can influence ice growth (see Karev et al. I., 2003; Karev et al. II., 2003; Makkonen, 2000 and references therein). The size and dynamics of the droplets are influenced by a number of parameters and physical phenomena, including aerodynamic drag, gravity, droplet collision, evaporation, and turbulence of the carrying phase. The effects of evaporation and cooling were discussed in Karev and Farzaneh (2002) leading to the conclusions drawn by this study, that evapora-

tion and cooling are the decisive factors in the determination of DSD, but that droplet collision and gravitational sedimentation are also significant under certain given conditions as predicted experimentally. Both the latter phenomena, therefore, are examined in detail in the present article and a two-dimensional model of laminar two-phase spray flows is presented. Calculations of droplet trajectories are based on a simple equation of droplet motion that considers aerodynamic drag and gravity as factors. The main goal of this study is to simulate the process of droplet collision and to study the way in which it influences DSD. Theoretical results are subjected to experimental verification, which is the rationale for the simulation of droplet motion in an icing wind tunnel. Ambient parameters are also adjusted so that the experiments approximate natural conditions as closely as possible. Since atmospheric icing processes are under examination here, water droplets are assumed to flow in the air stream. An ulterior goal of this study is that the model should include turbulence considering that it amplifies the effects of droplet collision on the DSD. There are several reasons for modeling the development of DSD in icing wind tunnels. Firstly, the collargol method (Godard, 1960), which was applied in earlier wind tunnel experiments (Karev and Farzaneh, 2002) to determine DSD, can be used only for ambient temperatures above the freezing point of water. In other words, it is not applicable under icing conditions. Moreover, it was found in Karev and Farzaneh (2002) that the DSD in an icing wind tunnel under various icing conditions was a strong function of the relative humidity of air. Thus, it was necessary to develop a method for the prediction of DSD under various icing conditions. Secondly, if the evolution of the DSD is known for a simulated aerosol cloud flowing inside the wind tunnel from the spray bar to the icing object, it is always possible to control the LWC/DSD combination near the icing object. By adjusting nozzle-dynamic

parameters (NDPs), experiments may be carried out with natural LWC/DSD combinations as recorded in field measurements. Lastly, the modeling of DSD development provides information about the non-uniformity of aerosol clouds. The droplet distribution in an aerosol cloud is not uniform in wind tunnels, while it can be considered uniform under natural conditions due to the large size of the aerosol cloud as compared to that of the icing object.

Considerable research has already been carried out on droplet collision. It is a widely accepted fact that binary droplet collisions exhibit five distinct regimes of outcomes, namely (i) coalescence after minor deformation, (ii) bouncing, (iii) coalescence after substantial deformation, (iv) reflexive separation, and (v) stretching separation. The collision process is usually characterized by three parameters: the Weber number, the impact parameter, and the droplet size ratio. Boundary curves between the regions of possible outcomes in terms of these parameters are proposed by several authors (Ashgriz and Poo, 1990; Brazier-Smith et al., 1972; Estrade et al., 1999). Extensive experimental investigation was conducted and several outcome maps are presented in Qian and Law (1997). Further experimental studies were reviewed by Orme (1997). Detailed description of each collision outcome regime is provided in Section 3 together with the boundary curves which are used in our model.

In the present paper, an attempt was made to simulate a two-phase air/dispersed water flow both numerically and experimentally. The initial DSD, LWC, and droplet velocities, as they occur at the nozzle outlet after the break-up of the emanating liquid jet, are determined by the properties of the liquid jet and the spray nozzle. The initial DSD is estimated in the computer simulation in accordance with previous experimental results. A two-dimensional model is derived to simulate droplet motion in the wind tunnel, and droplet trajectories

are modified according to collisions. The vertical distribution of the LWC near the icing object is also determined and verified by experimental observations.

2 Break-up Process

Several authors have studied the break-up process of liquid jets. Reitz and Bracco (1986) described, in detail, the mechanism of the break-up of round liquid jets. According to the linear stability theory, the liquid jet breaks up at the most unstable wave which is the one with the maximum growth rate. The corresponding dominant wavelength determines the mass mean diameter of the resulting droplets through the conservation of mass. Li (1995) proposed a model for finding the most unstable wave in cylindrical liquid jets. Lin and Reitz (1998) presented numerical formulas for the maximum growth rate and for the corresponding wavelength where liquid jets break up. These formulas provide an adequate approximation of the results discussed in Li (1995). Several empirically derived mean diameters for different types of nozzles are listed in Lefebvre (1989). One possible way of finding the resulting DSD is to compute the mass mean diameter or the median volume diameter and then apply a distribution function. Lefebvre (1989) reviewed some theoretical and empirical distribution functions that are widely used for DSD. Some of these functions give mass-based size distribution, but this can easily be converted into DSD, since droplets are assumed to be spherical. Experimental observations on the dependence of the mass-based size distribution on the NDPs are presented in Karev et al. (2002). DSD is recorded and the experimentally matched curve is obtained in Karev and Farzaneh (2002).

In a future study the median volume diameter will be determined by utilizing a

theoretical, numerical or empirical formula and a distribution function will be applied to estimate the DSD at the nozzle exit. Thus, the distribution obtained will not depend on the data measured or the actual experimental setting. The results obtained by Karev and Farzaneh (2002) are used as input in the present paper. These researchers measured DSD at the nozzle exit by using the collargol slide impact method (Godard, 1960). The description of these experiments can be found in Karev and Farzaneh (2002). Droplet diameters were measured, then these were collected in $5\,\mu$m-wide bins and their sizes were approximated by taking the arithmetic mean of each bin. In this paper, we simulate the flow for a particular set of measurements, where the NDPs were as follows: water pressure $p_w = 3.6 \cdot 10^5$ Pa, air pressure $p_a = 1.7 \cdot 10^5$ Pa, water flow rate $3.9 \cdot 10^{-6}\,\mathrm{m}^3/\mathrm{s}$, and air flow rate $3.7 \cdot 10^{-4}\,\mathrm{m}^3/\mathrm{s}$. The following curve was matched to the experimental results in Karev and Farzaneh (2002):

$$f(d) = \begin{cases} 0.0097\,(d-6.5)^2\,\mathrm{e}^{-0.1804d} & d \in [6.5\mu\mathrm{m}, 42.9\mu\mathrm{m}] \\ 0.0196\,(d-6.5)^2\,\mathrm{e}^{0.0012d^2-0.2483d} & d \in [42.9\mu\mathrm{m}, 100\mu\mathrm{m}] \end{cases}, \qquad (1)$$

where d is the droplet diameter. Droplets of a diameter in the range between $5\,\mu$m and $100\,\mu$m are observed near the nozzle outlets in the wind tunnel experiments. The proposed curve is not applicable without significant error if the droplet diameter is outside the range between $6.5\,\mu$m and $100\,\mu$m. In spite of the lower limit of this range, droplets of a diameter of less than $6.5\,\mu$m, but not less than $5\,\mu$m, may be considered. The reason for this is that the droplet size spectrum is discretized in the computation, $5\,\mu$m-wide bins are thereby created, and droplets in the $5\,\mu$m-to-$10\,\mu$m bin are treated as droplets of $7.5\,\mu$m in diameter. Also, since the diameter of the largest droplets in the present case is $100\,\mu$m, the upper limit of the range of applicability does not

cause any problem. In other experiments however, when the NDPs are changed and droplets of larger diameter are produced, the approximation represented by Equation (1) is not applicable. This justifies making a greater effort in our forthcoming research to find a workable formula which depends on NDPs, thereby making it applicable in the simulation of any experiment carried out using the same type of nozzle.

Figure 1 shows the DSD obtained in Karev and Farzaneh (2002) for the NDPs given in the previous paragraph. The diagram illustrates this by means of circles connected by a jointed line, while the dotted line represents the matched curve obtained by Equation (1). The DSD as obtained by Karev and Farzaneh (2002) may be used in this model as the initial DSD, in view of the fact that the simulated air/water flow in the wind tunnel assumes the same nozzle characteristics and NDPs as in the earlier experiments.

3 Droplet Collision

The binary droplet collision phenomenon is discussed in this section. The phenomenon of droplet collision is mainly controlled by the following physical parameters: droplet velocities, droplet diameters, dimensional impact parameter, surface tension of the liquid, and the densities and viscosity coefficients of the liquid and the surrounding gas, but further components may also be important, such as the pressure, the molecular weight and the molecular structure of the gas. From these physical parameters several dimensionless quantities can be formed, namely, the Weber number, the Reynolds number, impact parameter, droplet size ratio, the ratio of densities, and the ratio of viscosity coefficients. Thus, for a fixed liquid-gas system, the outcome of collisions can

be described by three non-dimensional parameters: either the Weber number or the Reynolds number, the impact parameter, and the droplet size ratio.

(i) The Weber number is the ratio of the inertial force to the surface force and is defined as follows:

$$We = \frac{\rho_d U_r^2 D_S}{\sigma}\,, \tag{2}$$

where ρ_d is the droplet density, U_r is the relative velocity of the interacting droplets, D_S is the diameter of the smaller droplet, and σ is the surface tension. In some references, the Weber number is based on the size of both droplets (Post and Abraham, 2002), i.e. the sum of the radii of the colliding droplets appears in Equation (2) instead of the diameter of the smaller droplet.

(ii) The dimensional impact parameter b is defined as the distance from the center of one droplet to the relative velocity vector placed on the center of the other droplet. This definition is illustrated in Figure 2. The non-dimensional impact parameter is calculated as follows:

$$B = \frac{2b}{D_L + D_S}\,, \tag{3}$$

where D_L is the diameter of the larger droplet.

(iii) The droplet size ratio is given by

$$\Delta = \frac{D_S}{D_L}\,. \tag{4}$$

It should be clear that $\Delta \leq 1$, although some authors prefer to use the reciprocal $\gamma = 1/\Delta$.

When two droplets interact during flight, five distinct regimes of outcomes may occur, as listed in Section 1, and depicted in Figure 3 in the $B - We$

plane for four different values of Δ. When two droplets approach each other, the gas layer between them becomes trapped and the pressure rises in the gap between the droplets. If the drops travel slowly enough then the gas has time to escape before the drops touch, so that coalescence can occur after minor deformation. This phenomenon is also referred to as slow coalescence in the literature (Post and Abraham, 2002). Regime I in Figure 3 corresponds to this outcome. If the relative velocity of the droplets is higher, there is not enough time for the gas to escape and the surfaces of the droplets do not make contact due to the intervening gas film, so the droplets become deformed and bounce apart. The corresponding domain in Figure 3 is regime II. When the relative velocity is even higher and the collisional kinetic energy is sufficient to expel the intervening layer of gas, the droplets will coalesce after substantial deformation. Regime III in Figure 3 is associated with coalescence after substantial deformation. The film thinning process and the effect of surface mobility on collision are examined in detail in MacKay and Mason (1963), and Jeelani and Hartland (1998), respectively. If the collisional kinetic energy exceeds the value for permanent coalescence, then the temporarily coalesced droplets separate into two or more droplets. Qian and Law (1997) distinguish two regimes of separation, i.e. coalescence followed by separation for near head-on collisions, and coalescence followed by separation for off-centre collisions. The droplets oscillate and undergo a reflexive separation for near head-on collisions (regime IV in Figure 3), while they tend to stretch apart and undergo a stretching separation for off-centre collisions (regime V in Figure 3). Temporary coalescence (regimes IV and V) may result in either disruption or fragmentation. In disruption, the collision product separates into the same number of droplets which existed prior to the collision. In fragmentation, the coalesced droplet breaks up into numerous satellite droplets (Orme, 1997).

It is clear that bounce affects droplet trajectory, but it does not modify the droplet size. Coalescence followed by disruption does not have any significant influence on droplet size. Even if some mass transfer occurs, the droplet diameters are not usually changed in any observable way. Other regions of collision outcomes, however, may influence DSD, because the sizes of post-collision droplets are different from those of the pre-collision droplets. During fragmentation, a number of small satellite droplets is formed with the accompanying decrease in droplet size. Fragmentation occurs when the relative velocity of colliding droplets is high, and since low velocity flows are under examination here, the phenomenon almost never occurs in this investigation. Coalescence after either minor or substantial deformation results in one droplet of a larger size than that of the pre-collision droplets. Since these phenomena appear at low velocities, it is expected that their effect is significant as regards this study indicating that droplet collision causes an increase in droplet size.

In the next subsections, boundary curves between the regimes of possible outcomes are derived in terms of the dimensionless parameters introduced above. These curves are signified by capital letters in Figure 3.

3.1 Stretching Separation and Coalescence

Brazier-Smith et al. (1972) proposed a stretching separation criterion based on energy consideration. The criterion for stretching separation is that the rotational energy of the coalesced droplet exceeds the surface energy required to re-form the original two droplets from the coalesced pair, which implies the

following:

$$We > \frac{4.8}{B^2}\frac{\left[1+\gamma^2-\left(1+\gamma^3\right)^{2/3}\right]\left(1+\gamma^3\right)^{11/3}}{\gamma^6\left(1+\gamma\right)^2}\,. \tag{5}$$

Curve A in Figure 3 represents this condition. Ashgriz and Poo (1990) proposed an alternative criterion for stretching separation which is assumed to arise when the total effective stretching kinetic energy is greater than the surface energy of the region of interaction. They showed, however, that condition (5) also provides a satisfactory prediction for the stretching separation boundary. The velocity of each droplet after stretching separation is provided in Gavaises et al. (1996) as follows:

$$U_L^{new} = \frac{U_L D_L^3 + U_S D_S^3 + D_S^3\left(U_L - U_S\right)Z}{D_L^3 + D_S^3}\,, \tag{6}$$

where U_L and U_S are the velocities of the larger and smaller pre-collision droplets, respectively, and

$$Z = \frac{B - B_{cr}}{1 - B_{cr}}$$

in which B_{cr} is the critical impact parameter above which the collision results in stretching separation and below which the coalescence is permanent. This parameter may be computed according to the following formula

$$B_{cr} = \min\left(1.0, \sqrt{\frac{4.8}{We}\frac{\left[1+\gamma^2-\left(1+\gamma^3\right)^{2/3}\right]\left(1+\gamma^3\right)^{11/3}}{\gamma^6\left(1+\gamma\right)^2}}\right). \tag{7}$$

The velocity U_S^{new} of the smaller droplet may be calculated similarly, in view of the fact that the quantities designating the larger and the smaller droplets are interchanged in Equation (6).

3.2 Reflexive Separation and Coalescence

Ashgriz and Poo (1990) derived a criterion for reflexive separation. This is based on a balance between reflexive kinetic energy and surface energy. They consider that once the coalesced drops have stretched far enough for a thin ligament to form, the surface energy will promote the separation rather than prevent it. Therefore, the reflexive kinetic energy need not be so high as the nominal surface energy for separation to occur. They postulate that the condition of reflexive separation is that the effective reflexive kinetic energy be more than 75 % of the nominal surface energy which can be expressed as follows:

$$We > 3\left(7\left(1+\Delta^3\right)^{2/3} - 4\left(1+\Delta^2\right)\right)\frac{\Delta\left(1+\Delta^3\right)^2}{\Delta^6\eta_1+\eta_2}, \tag{8}$$

where

$$\eta_1 = 2\left(1-\xi\right)^2\left(1-\xi^2\right)^{1/2} - 1, \quad \eta_2 = 2\left(\Delta-\xi\right)^2\left(\Delta^2-\xi^2\right)^{1/2} - \Delta^3 \quad \text{and}$$

$$\xi = \frac{1}{2}B\left(1+\Delta\right).$$

The corresponding transition curve in Figure 3 is the one indicated by B.

3.3 Bounce and Coalescence

Estrade et al. (1999) provide a criterion for bouncing. They assume that if the droplet initial kinetic energy of deformation does not exceed the energy required to produce a limit deformation, then droplets will bounce. The criterion required for coalescence to occur is given by

$$We > \frac{\Delta\left(1+\Delta^2\right)\left(4\phi'-12\right)}{\chi\left(1-B^2\right)}, \tag{9}$$

where

$$\chi = \begin{cases} 1 - (2-\tau)^2 (1+\tau)/4, \text{ if } \tau > 1.0 \\ \\ \tau^2 (3-\tau)/4, \qquad\qquad \text{if } \tau \leq 1.0 \end{cases}, \quad \tau = (1-B)(1+\Delta)$$

and ϕ' is the shape factor. This factor is a measure of the deformation of the droplets from their initial spherical shape, and its proposed value is 3.351. Curve C in Figure 3 is defined by condition (9).

3.4 A Composite Collision Outcome Model

This composite collision outcome model takes account of stretching separation, reflexive separation and bounce, as well as coalescence after minor deformation (or slow coalescence) and coalescence after substantial deformation. Since there is no criterion proposed in the literature for slow coalescence to occur, experimental results (Qian and Law, 1997) are considered in order to apply a simple condition. We use the fact that droplet bounce is not observed in water droplets for head-on collisions at atmospheric pressure, and also that the regime of slow coalescence always vanishes as the non-dimensional impact parameter reaches unity. The boundary curve in the $B - We$ plane is the line joining two given points (see curve D in Figure 3). One of these points separates the regime of bounce from that of coalescence after substantial deformation for head-on collisions, while the other point is the one where the Weber number is zero and the impact parameter is unity. This implies that the transition curves between slow coalescence and bounce (curve D), as well as between bounce and coalescence after substantial deformation (curve C), intersect each other for $B = 0$. As the droplet size ratio, Δ, decreases, separation

occurs for higher Weber numbers only, while the regimes of slow coalescence and bounce shrink so that the regime of coalescence after substantial deformation becomes larger. Note that the regime of slow coalescence does not disappear for $\Delta = 0.25$, but it is not visible due to the scale in Figure 3(d).

Qian and Law (1997) presented the results of a comprehensive experimental investigation of binary droplet collision dynamics with emphasis on the transition between different collision outcomes. They carried out numerous experiments involving different liquids, different environments and different gas pressures, and they also produced photographic images of the processes under examination. According to their experimental results, the ambient gas pressure affects the location of the boundary curves. If the gas pressure is low, then droplet bounce occurs only for large impact parameters, i.e. the transition curves C and D intersect each other in certain cases of $B > 0$, while the regions of coalescence after minor and substantial deformation are not distinct. On the other hand, if the gas pressure is high, then transition curve C moves toward higher Weber numbers, while the transition curve D moves in the opposite direction. Thus, if the gas pressure increases, then the region of slow coalescence tends to shrink or even disappear. All the experimental results revealed in Qian and Law (1997) show good qualitative agreement with the regimes of outcomes and the transition between them obtained by the conditions presented in this section. Their results for water droplets in a nitrogen environment at a gas pressure of around $2 \cdot 10^5$ Pa coincide entirely with our collision regimes even from a quantitative point of view.

The composite model is applied during droplet flow in the wind tunnel beginning at least 30 cm downstream of the nozzle exit where the disintegration of the liquid jet is assumed to be completed. It is important to emphasize

this fact, because the composite collision outcome model is not constructed with the intention of simulating the break-up process, and the assumption of the model that the velocity of droplets is low, i.e. in the range of free stream velocity, is applicable only when the process of atomization is already over. The droplet size ratio, the Weber number, and the impact parameter are all calculated during simulation of the droplet motion. Firstly, it is necessary to ascertain whether slow coalescence occurs by using the boundary condition between the regions of slow coalescence and bounce, as explained earlier in this subsection. Then criterion (9) is applied to determine whether or not bouncing has occurred. If bounce has not occurred, then droplets coalesce, at least temporarily. Lastly, criteria (5) and (8) are applied to determine if either stretching separation or reflexive separation has occurred. After obtaining the collision outcome, the sizes and velocities of the post-collision droplets need to be determined. In case of coalescence, the size and velocity are calculated in such a way as to conserve mass and momentum. When droplets bounce, their sizes do not change and their velocities are modified according to the conservation of momentum. If separation occurs, the sizes of post-collision droplets are assumed to be equal to those of the pre-collision droplets. Although Ashgriz and Poo (1990), in their study, found that there was a mass transfer from the larger droplet to the smaller one, they did not publish any quantitative analyses at that time. The velocities of post-collision droplets, in the case of stretching separation, are calculated according to the relation given by (6), while in the case of reflexive separation they are approximated by the velocities of the pre-collision droplets. According to the low velocities and Weber numbers of the simulated flows, separation appears rarely as compared to the other three regions of outcomes. Since fragmentation is the result of collision with excessive kinetic energy and consequent high Weber number,

satellite droplet formation is not considered in our model. A composite model was proposed by Post and Abraham (2002) also, and although they did not investigate slow coalescence, they studied Diesel spray with high velocities and Weber numbers, thus the appearance of slow coalescence in their work may be disregarded. In contrast, the present model deals with flows with lower velocities where the occurrence of slow coalescence is far more significant.

4 The Two-Dimensional Model

The two-dimensional model for air/dispersed water flows is based on the particle-source-in cell (PSI-CELL) model constructed by Crowe et al. (1977) and the droplet equation proposed by Maxey and Riley (1983). The flow field is subdivided into a series of cells, which are regarded as control volumes. For simplification, it is assumed that the cross-section of the wind tunnel is constant, as are gas velocity and pressure. The liquid phase is treated in a Lagrangian fashion. Since there are too many droplets to examine individually, they are collected into parcels. The method is based on the concept of the discrete parcel approach (O'Rourke and Bracco, 1980). Each parcel contains the same number of drops of identical size and velocity. The trajectories of the droplets are obtained by integrating the equations of motion for the droplets in the gas flow.

The equation of motion of a droplet with simplifications according to the assumptions of the previous paragraph is given by Maxey and Riley (1983)

$$\frac{\pi}{6}d^3\left(\rho_d + 0.5\rho\right)\frac{\mathrm{d}\mathbf{v}}{\mathrm{d}t} = \frac{\pi}{6}d^3\left(\rho_d - \rho\right)\mathbf{g} + 3\pi d\mu f\left(\mathbf{u} - \mathbf{v}\right) , \tag{10}$$

where $\mathbf{v}, \mathbf{u}$ and $\mathbf{g}$ are the droplet velocity, gas velocity, and gravity vectors, respectively, d and ρ_d are the diameter and density of the droplet, respectively, ρ and μ are the density and dynamic viscosity of the gas, respectively, while f considers the Stokes drag, expressed as follows (Crowe et al. (1977)):

$$f = 1 + 0.15Re^{0.687} \tag{11}$$

for all Reynolds numbers Re up to 1000, based on the gas-droplet relative velocity

$$Re = \frac{\rho \left|\mathbf{u} - \mathbf{v}\right| d}{\mu} . \tag{12}$$

Dividing Equation (10) by $(\rho_d + 0.5\rho)\pi d^3/6$, and assuming that $\rho_d \gg \rho$, which is held in the present study, because the density of water is much greater than that of air, we obtain

$$\frac{\mathrm{d}\mathbf{v}}{\mathrm{d}t} = \mathbf{g} + \frac{18\mu}{\rho_d d^2} f \left(\mathbf{u} - \mathbf{v}\right) . \tag{13}$$

This equation is transformed into dimensionless form for the sake of simplicity throughout the discussion. The nondimensional parameters $\mathbf{U} = \mathbf{u}/u, \mathbf{V} = \mathbf{v}/u$ and $T = tu/l$ are used, where $u = |\mathbf{u}|$ and l is the horizontal distance between the nozzles and the icing object in the tunnel or, in other words, the simulated length of the tunnel. Thus, T means the time required for a droplet to pass through the tunnel if the horizontal component of its velocity were always the air stream velocity u. The introduction of these parameters leads to the following equation:

$$\frac{\mathrm{d}\mathbf{V}}{\mathrm{d}T} = \frac{l}{u^2}\mathbf{g} + \frac{18\mu l}{\rho_d d^2 u} f \left(\mathbf{U} - \mathbf{V}\right) . \tag{14}$$

Since f is a function of the Reynolds number, which depends on the droplet velocity and, thereby, f varies with time, Equation (14) is integrated numerically by using the Euler scheme in a predictor-corrector mode:

$$\mathbf{V}_* = \mathbf{V}_j + \left.\frac{\mathrm{d}\mathbf{V}}{\mathrm{d}T}\right|_j \Delta T\,, \tag{15}$$

$$\mathbf{V}_{j+1} = \mathbf{V}_j + \left(\left.\frac{\mathrm{d}\mathbf{V}}{\mathrm{d}T}\right|_j + \left.\frac{\mathrm{d}\mathbf{V}}{\mathrm{d}T}\right|_* \right) \frac{\Delta T}{2}\,, \tag{16}$$

where ΔT is the nondimensional time interval, and the subscripts j and $j+1$ refer to quantities at the beginning and at the end of the time increment, respectively. The subscript $*$ refers to an intermediate value, which is the result of the predictor step represented by Equation (15), and which is corrected in the corrector step represented by Equation (16). After determining the new droplet velocity $\mathbf{V}_{j+1}$, the new droplet position $\mathbf{X}_{j+1}$ is obtained by applying the trapezoidal scheme

$$\mathbf{X}_{j+1} = \mathbf{X}_j + (\mathbf{V}_j + \mathbf{V}_{j+1}) \frac{\Delta T}{2}\,, \tag{17}$$

where the droplet position with horizontal component X and vertical component Y are also nondimensionalized by the characteristic length l, i.e. the simulated length of the wind tunnel. Note that Equation (17) represents simpler computation than Equations (15) and (16), but it cannot be applied to find droplet velocity, because $\mathrm{d}\mathbf{V}/\mathrm{d}T|_{j+1}$ is not known when $\mathbf{V}_{j+1}$ is computed.

The parcels of drops are tracked in space and time as if they were a single droplet only, but from the collisional point of view, their size is considered larger according to the number of droplets carried in one parcel. In each time step, the position and velocity of droplet parcels are determined, and if the dis-

tance between two parcels is less than the sum of their radii, they will collide. The outcome of collisions and the sizes and velocities of post-collision droplets are determined by utilizing the composite collision outcome model described in Subsection 3.4. Then, this process is continued in the next time steps until a termination condition is not satisfied, in other words, until droplets do not reach the icing object or the end of the wind tunnel.

5 Results and Discussion

A Fortran computing tool was written to calculate the positions and velocities of parcels of droplets in the wind tunnel, as well as sizes of droplets after collision according to the models described in Subsection 3.4 and Section 4. First, an individual droplet is tracked in order to study the effect of gravity on droplet motion. Then, numerous droplets are considered and collected into parcels, their motion is simulated and the way in which their collisions influence the DSD is examined.

5.1 Effects of Gravity on Droplet Motion

It is assumed, for this analysis and discussion, that a water droplet flows in air and the temperature of the air is $-20\,^{\circ}\mathrm{C}$. Note that, in the present model, the only role of temperature is that the density and viscosity of the ambient gas are determined by its temperature. The process of droplet collision and coalescence is assumed to be independent of gas temperature. However, a later improvement of the model will include evaporation, in which air temperature plays an important role. Thus, the air temperature does not have a signifi-

cant influence on the present simulation results, but it is chosen in accordance with the conditions of the LWC measurement. The densities of the gas and the droplet are $\rho = 1.39\,\mathrm{kg/m^3}$ and $\rho_d = 1000\,\mathrm{kg/m^3}$, respectively, the dynamic viscosity of the gas is $\mu = 1.62 \cdot 10^{-5}\,\mathrm{kg/(ms)}$ and the gravitational acceleration is $g_x = 0\,\mathrm{m/s^2},\ g_y = -9.81\,\mathrm{m/s^2}$. The initial droplet velocity is $v_{x,0} = 20\,\mathrm{m/s},\ v_{y,0} = 0\,\mathrm{m/s}$ and the gas velocity is assumed to be horizontal. The dimensionless parameters introduced in Section 4 are used throughout this discussion. The effect of free stream velocity and droplet diameter on the droplet trajectory and droplet velocity is investigated in terms of the Froude number, Fr, and the Stokes number, St, which are defined as follows:

$$\begin{aligned} Fr &= \frac{u^2}{|g_y| l}\,, \\ St &= \frac{\rho_d d^2 u}{18 \mu l}\,. \end{aligned} \tag{18}$$

The droplet trajectory was simulated assuming that the droplet moves in a wind tunnel 4.4 m and 0.45 m in simulated length (l) and height (h), respectively. Thus, $X = 0$ and $X = 1$ represent the horizontal position of the nozzles and the icing body or the end of the tunnel, respectively, while $Y = 0,\ Y = -0.051$, and $Y = 0.051$ correspond to the vertical position of the nozzles, the bottom of the tunnel and the top of the tunnel, respectively. The wind tunnel is described in greater detail in Section 6. Figure 4 shows the droplet position as the Froude and Stokes numbers are varied. According to Figure 4(a) if the Froude number increases, then the effect of gravity decreases, i.e. the vertical deflection of the droplet trajectory is less. On the other hand, if the Stokes number increases, then the effect of gravity is more significant, the vertical deflection of the droplet trajectory is greater, as shown in Figure

4(b). The Froude number increases with free stream velocity, although the droplet diameter decreases slightly, because the Stokes number should be kept constant in Figure 4(a). The Stokes number increases with droplet diameter, and the free stream velocity is constant in order for the Froude number to remain constant in Figure 4(b). These relationships mean that the influence of gravity is greater for lower air velocities and larger droplet diameters.

Figure 5 shows the horizontal and vertical components of the dimensionless droplet velocity, as the Froude and Stokes numbers are varied. It can be observed in Figures 5(a) and 5(b) that the horizontal component of the droplet velocity tends toward a limit, which is the air stream velocity. If the Froude number increases or the Stokes number decreases then the rate of convergence is faster. According to Figures 5(c) and 5(d), the magnitude of the vertical component of the droplet velocity decreases with the Froude number and increases with the Stokes number, which corresponds to the fact that the effect of gravity decreases with air stream velocity and increases with droplet diameter.

The vertical deflection of droplet trajectories influences the vertical distribution of LWC. Here, we consider a flow of droplets and simulate their motion under the same conditions as given in the first paragraph of this subsection, except that the droplet velocity is assumed to have a vertical component due to the non-zero spray angle of the nozzle. This component is varied periodically between a minimum and a maximum value such that the angle of the velocity vector is in the interval $(-\alpha/2, \alpha/2)$, where α is the spray angle. The spray angle is a property of the nozzle and is thus known. The simulation starts 30 cm downstream of the nozzles for air stream velocity 30 m/s and 50 cm downstream of the nozzles for air stream velocities 5 and 10 m/s. The wind tunnel is divided into small cells and the LWC is computed in the cells that

are located at the icing object or at the end of this tunnel. The position and size of each droplet are known at the end of simulation, thus, the total mass of droplets can be computed in each cell. The mass of droplets in the cell at $Y = 0$, or in an adjacent cell, divided by the volume of the cell gives a reference LWC that is indicated by LWC_0 in what follows. Then the ratio of LWC in the other cells to LWC_0 provides a vertical distribution of the LWC. Since this computed relative LWC is compared to experimental results in Section 6, and the measured relative LWC is based on the amount of ice on a cylinder, the number of droplets in each cell must be multiplied by the collection efficiency. The collection efficiency is different for droplets of different diameters, and Section 6 provides a discussion of how to compute this parameter.

Figure 6 shows the ratio of the LWC in the actual cell to LWC_0 for three different air stream velocities. For a high velocity (30 m/s), droplets can be found in a very narrow region only, i.e. droplets do not appear more than 5 cm above the zero vertical coordinate ($Y = 0.011$) and they do not appear more than 8 cm below this level either ($Y = -0.018$). The lower the air stream velocity is, the larger this region becomes. For 10 m/s, droplets are found 7 cm above ($Y = 0.016$) and 20 cm below the level of the nozzles ($Y = -0.045$), while droplets occur even at the bottom of the tunnel, i.e. 22.5 cm below the level of the nozzles ($Y = -0.051$), if the air stream velocity is 5 m/s only. The maximum LWC also occurs at a lesser height as the air stream velocity decreases. It may be concluded that the effect of gravity is negligible for high air stream velocities, while for low air stream velocities it has a significant influence on the droplet trajectory and the vertical distribution of the LWC.

5.2 Effects of Droplet Collision on Droplet Size Distribution

Parcels of droplets emanating from a nozzle into the wind tunnel are examined for this assessment. As discussed in Section 2, the flow rate of the emanating water may be adjusted to requirements. Since the geometry of the nozzle is known, the initial droplet velocity may be calculated. The vertical component of the droplet velocity is determined as discussed in Subsection 5.1.

The initial DSD is determined by the experimental results as discussed in Section 2. From a computational point of view, the droplet spectrum is first discretized. The points on the jointed line in Figure 1 represent the relative frequencies of the appearance of droplets in each bin, and these values are then used to obtain the discrete droplet spectrum. An interval of random numbers corresponds to every discrete value of the droplet diameter as explained in what follows. The relative frequency of droplets in the first bin, f_1, determines the interval $i_1 = [0, f_1)$, the relative frequency of droplets in the second bin, f_2, determines the interval $i_2 = [f_1, f_1 + f_2)$, and so on, while the relative frequency of droplets in the last bin, f_n, determines the interval $i_n = [f_1 + f_2 + \ldots + f_{n-1}, f_1 + f_2 + \ldots + f_n) = [f_1 + f_2 + \ldots + f_{n-1}, 1)$. Thus, each random number in the interval $[0, 1)$ is an element of exclusively one of the intervals $i_1, i_2, \ldots, i_n$. Then, a random number is generated for each parcel of droplets and the diameter of each droplet in the parcel is the value in the spectrum that corresponds to the interval of which the random number is an element. The solid line in Figure 7 represents the DSD at the nozzle exit. Since the droplet spectrum is discretized and droplet diameters are based on a limited number of measured droplet diameters, the resulting distribution function is not smooth, it even oscillates in some regions. Note that using a smooth matched function

and generating a large quantity of random numbers, thereby taking numerous parcels into account, would contribute to avoiding this problem, but it would also increase the computational costs.

The number of emanating droplets in unit time is determined by the water flow. If the volume mean diameter is known, the number of droplets per unit volume may be calculated. If this number is multiplied by the water flow, the number of emanating droplets may be obtained.

In the computer simulations, we assume that the nozzle exit diameter is $a = 6 \cdot 10^{-4}$ m and the spray angle is $\alpha = 15^{\text{o}}$. The air stream velocity is $u = 10$ m/s and horizontal. The horizontal component of the initial droplet velocity is $v_{x,0} = 20$ m/s. The simulated length of the wind tunnel is 4.4 m. The DSD of the emanating droplets and the DSD at the end of simulation ($t = 1.55$ s or $T = 3.52$) is shown in Figure 7. In order that the two curves be clearly distinguishable in the domain of large droplets the same distributions are enlarged in this figure. The initial and final median volume diameters are 37.9 μm and 45.5 μm, respectively.

In Figure 8, the change in the number of droplets of certain diameters over time is shown for air stream velocity $u = 10\,\text{m/s}$. Four diameters, 10 μm, 20 μm, 40 μm, and 60 μm, in particular, were chosen. Here, bins with a width of 10 μm were used, thus diameter 10 μm indicates droplets of a diameter between 5 μm and 15 μm. The number of small droplets decreases due to coalescence when two droplets form a single droplet of a larger diameter. The number of droplets of diameter $d = 10\,\mu$m decreases by 18 %. The rate of decrease for droplets of diameter $d = 20\,\mu$m is 12 %. The number of droplets of a 40 μm diameter changes to a slight degree, decreasing by less than 7 %, although during

the simulation the number of droplets changes several times. The explanation for this result is that the number of droplets of this diameter that coalesce and form larger droplets as well as the number of coalescences that result in droplets of 40 μm diameter are approximately the same. The number of droplets of 60 μm diameter increases by 15 %. Although the curves representing the initial and final DSDs in Figure 7 are closely similar to each other, the decrease in the number of small droplets combined with the increase in the number of large droplets results in a not negligible increase in the median volume diameter which may even exceed 20 %.

It should be noted that the changes in the curves in Figure 8 are more significant at the beginning of the simulation, while the number of droplets of each diameter is more or less stabilized at the end of the simulation. The explanation for this fact is that droplets are closer to each other, therefore the number of collisions and coalescences are higher at the outset. It should also be noted that several steps may be observed in the curves in Figure 8. The reason for these steps is that the process of droplet coalescence is discrete. Once two droplets coalesce, they disappear from the simulation and another droplet of a larger diameter substitutes itself for them. The steps have finite tangents in the figures, because droplets are counted in discrete time steps only (which are larger than those of the simulation), therefore, the change in their number is not considered immediately at the moment of coalescence. Also, it is only possible to notice that the steps are higher if the diameter of the droplet is large, because the initial number of these droplets is much lower. Since each parcel contains the same number of droplets, and coalescence means that all the droplets in the parcels coalesce, one collision which results in coalescence causes a significantly greater change in the number of large droplets than in

the number of small droplets.

These results show that droplet size increases due to droplet collision and coalescence even in laminar flow. The flow in the wind tunnel, however, is turbulent and we expect that the effect of collision is greater in turbulent flow, because the relative velocity of colliding droplets is usually higher. A further goal of this work, therefore, is to develop the present model to include turbulence and to study how droplet size varies due to the phenomenon of collision in turbulent flow.

6 Validation of Simulation Results

A number of experiments were carried out in the wind tunnel which is described in Subsection 6.1. The relative LWC along the vertical direction was measured. Since measurement results are based on the amount of ice accreted on a cylinder, it must be considered that the ratio of droplets that hit the cylinder depends on the droplet size and is less than unity. The calculation of the collection efficiency that describes this ratio is discussed in Subsection 6.2. Our model is mainly constructed in order to simulate the effect of gravity and the evolution of DSD, but it is also applicable for computing relative LWC as is discussed in Subsection 5.1. Since the DSD influences the LWC and gravity affects the vertical distribution of LWC, the model is validated by comparing computed and measured relative LWC along the height of the tunnel at the location of the icing object. Simulation and experimental results are compared in the last subsection of this section.

6.1 The Experimental Set-up

Atmospheric icing processes can be modeled by wind-tunnel experiments. The CIGELE icing research tunnel is a closed-loop low-speed icing wind tunnel with a total length of about 30 m, including a 3 m long test section with a rectangular cross-section 0.45 m high and 0.9 m wide. The technique for simulating the atmospheric icing process is to inject water into a cold air stream through the nozzles located on a horizontal spray bar. The spray bar is located just downstream from the honeycomb, 4.4 m upstream from the middle of the test section, where the icing structure being analyzed is usually placed (see Figure 9). The pressures and the flow rates of the water line and air line, i.e. the NDPs may be adjusted to requirements. These parameters together with the nozzle characteristics have an influence on the liquid jet break-up into a number of droplets, and they determine the resulting DSD. For a more detailed description of the wind tunnel used for this sequence of experiments see Karev and Farzaneh (2002).

6.2 The Collection Efficiency

The computed and measured relative LWC along the vertical direction are compared in the following subsection. Cylinders are used as icing objects in these experiments, and the relative LWC is computed by using the amount of ice accreted on the cylinder (a more detailed discussion may be found in Subsection 6.3). In the computations, it must be considered that air streamlines are deflected around the icing object, and small droplets tend to follow them, hence the ratio of particles that hit the icing object must be reduced from

unity. If the icing object is cylindrical then this ratio, the collection efficiency, can be parameterized by two dimensionless parameters

$$K = \frac{\rho_d v d}{9\mu D}\,, \tag{19}$$

where D is the cylinder diameter, and

$$\Phi = \frac{Re_d^2}{K}\,, \tag{20}$$

where the Reynolds number, Re_d, is based on the free stream velocity. The equations of droplet motion in the airflow around a cylinder can be solved numerically (Langmuir and Blodgett, 1945), and the collection efficiency, ϵ, may be determined by using the following empirical fit to the numerically calculated data (Finstad et al., 1988 and Makkonen, 2000)

$$\epsilon = A - 0.028 - C(B - 0.0454), \tag{21}$$

where

$$A = 1.066K^{-0.00616}\mathrm{e}^{-1.103K^{-0.688}}, \tag{22}$$
$$B = 3.641K^{-0.498}\mathrm{e}^{-1.497K^{-0.694}}, \tag{23}$$
$$C = 0.00637(\Phi - 100)^{0.381}. \tag{24}$$

According to this formula, the collection efficiency, ϵ, can be determined for any droplet diameter, and, in the computation of relative LWC, the number of droplets of each bin of diameters is multiplied by the corresponding collection efficiency in order to obtain the amount of droplets that accrete on the icing object.

6.3 Computed and Measured Relative LWC

Experiments were carried out in the CIGELE icing research tunnel and were subsequently compared with the results of computer simulation in Figure 11. Cylinders are placed at a distance of 4.4 m from the nozzle, at seven different levels, i.e. at a height of +15, +10, +5, 0, -5, -10 and -15 cm each, where the 0 height is the level of the nozzles. Only two cylinders are used in each experiment, and are situated 10 cm apart in order to minimize their mutual influence. The cylinders are exposed to air/dispersed water flow for two minutes, then the circumferences of the cylinders covered by ice are measured every 10 cm along the length of the cylinder. The difference between the circumferences of the cylinders with and without ice makes it possible to compare the quantity of ice on the cylinders at different locations and at different heights, and also to calculate the local relative LWC (Ide, 1990). A cylinder covered by ice at the end of the experiment is shown in Figure 10.

Experiments were performed for fixed NDPs which were given in Section 2, and for air stream velocities of 5 m/s, 10 m/s, and 30 m/s. The NDPs determine the DSD at the nozzle exit as shown by the jointed line in Figure 1, with an MVD of 37.9 μm. The LWC depends on the NDPs and also on the air stream velocity. This LWC was 2.9 g/m^3, 5.0 g/m^3 and 7.7 g/m^3 for air stream velocities of 5 m/s, 10 m/s and 30 m/s, respectively, at the mid-point of the cross-section. The temperature was set at -20 °C, but some oscillations with an amplitude of about 2 °C could not be avoided. The relative humidity was between 75 % and 90 % during the experiments.

Experimental results are given in Figure 11(a), 11(b) and 11(c), respectively.

Steps present the relative LWC according to our calculations, while points correspond to experimental results. Circles, stars and plus signs show results of measurements in the middle of the cross section of the tunnel, 10 cm right and left of the center, respectively. In a similar fashion to Figure 6, the ratio of the actual LWC to LWC_0 is presented in these figures. It may be seen that the region where droplets appear is wider for lower air stream velocity in both the computer simulation and the experiment. The model provides an acceptable estimation of the relative LWC for an air stream velocity of $u = 5$ m/s, although an underestimation may be observed above the level of the nozzles. Since the change between the regions where there are no droplets and where the amount of droplets has reached a maximum is slightly more abrupt as observed in the experiments, the relative LWC is underestimated near the top and bottom of the tunnel, for $u = 10$ m/s. The difference between these changes is more noticeable for $u = 30$ m/s. The LWC maxima in both theoretical and experimental investigations appear farther from the zero height for lower air stream velocity. It should be noted that abrupt jumps appear in Figures 11(a)-11(c). The vertical distribution of LWC would have been smoother if the number of parcels included in the simulation increased, but causing this flattening out would also result in a considerable increase in the computational costs. It should be noted also, that even the errors in measurement may be considered to be within the same range as the abrupt jumps. Thus, it may be concluded that both simulation and experimental results are qualitatively the same, but the model tends to underestimate the number of droplets, and thereby the LWC, as the air stream velocity increases. One reason for this disparity is that turbulence has a significant influence on the flow and it is not considered in the computations. Droplets are dispersed in the air flow due to turbulence, therefore the effects of turbulence on the spray particles

are often modelled by adding a fluctuating velocity to the droplet velocity. Turbulence causes the appearance of the dispersed phase in a wider vertical range, as observed in the experiments, and it may also amplify the effects of droplet collision by increasing the relative velocity of colliding droplets. A further explanation of the disagreement between the theoretical and experimental results may be the fact that in the theoretical calculations here, evaporation and cooling are not taken into account since they are outside the scope of the present work. In a previous study (Karev and Farzaneh, 2002), however, these factors were found to be significant when the relative humidity of air was less than 70 %.

7 Conclusions

A theoretical model of a two-phase air/dispersed water spray flow was constructed. In particular, an icing wind-tunnel experiment was simulated, whereby water flow emanates from an air-assist nozzle at which point the water jet breaks up into droplets. The break-up process determines the initial DSD. This distribution was computed on the basis of the data measured, while the computer simulation of the flow in the wind tunnel provided the final DSD.

This model considers droplet collision and gravitational sedimentation in that they influence droplet motion. Simulations show that the effect of gravity, i.e. the vertical deflection of droplet trajectories, is more pronounced when the Froude number is lower and the Stokes number is higher, i.e. when the droplet size is larger or the air stream velocity is lower. For low air stream velocities such as 5 - 10 m/s, the vertical deflection of droplet trajectories is significant, especially for large droplets. This causes the droplets to appear

in a wider region below the level of the nozzles and the maximum of the LWC occurs at a lower height than in the case of higher air stream velocities. Experimental observations support simulation results qualitatively, although the model underestimates the dispersion of droplets for higher air stream velocities. In a future study, the effects of evaporation and turbulence will be scrutinized in the expectation of improving the model.

Droplet collision and coalescence affect droplet size. According to simulation of droplet motion at a distance of 4.4 m between the spray bar and the icing body, the number of small droplets decreases and that of the large droplets increases significantly. The number of droplets of 20 μm diameter decreases by around 12 %, while the number of droplets of 10 μm diameter may decrease by as much as 20 %. In previous investigations (Karev and Farzaneh, 2002) it was found that the influence of evaporation and cooling was also the most significant on droplets of small diameter (less than 15 μm), and when the relative humidity of air was less than 70 %, these droplets may even evaporate completely. The number of droplets of 40 μm diameter decreases by about 7 %, but droplets of 60 μm diameter may increase by close to 15 %. According to these changes in droplet size, the median volume diameter may increase by 20 % due to coalescence, assuming that the flow is laminar. These results show that evaporation and cooling are not the only effects which are capable of changing droplet size and trajectory, but that droplet collision and coalescence are also important, together with gravitational sedimentation, which can be considerable under certain conditions. Furthermore, there is a significant difference between the effect of evaporation and the effect of droplet coalescence. The number of droplets of any diameter decreases due to evaporation, albeit the rate of decrease is much lower for large droplets. However, only the number

of small droplets decreases due to collision followed by coalescence, while the number of large droplets increases. The importance of the final DSD and the droplet trajectories in icing processes is that, together with the geometry of the icing object and the air stream velocity, they determine the efficiency of collisions between the droplets and the icing object, as well as the amount of ice accreted on the icing object.

Acknowledgments

This research was carried out within the framework of the NSERC/Hydro-Québec Industrial Chair on Atmospheric Icing of Power Network Equipment (CIGELE) and the Canada Research Chair on Atmospheric Icing Engineering of Power Network (INGIVRE) at the University of Québec at Chicoutimi. The authors would like to thank all the sponsors of the CIGELE for their support.

References

Ashgriz, N., Poo, J. Y., 1990. Coalescence and separation in binary collisions of liquid drops. Journal of Fluid Mechanics 221, 183-204.

Brazier-Smith, P. R., Jennings, S. G., Latham, J., 1972. The interaction of falling water droplets: coalescence. Proceedings of the Royal Society of London A 326, 393-408.

Crowe, C. T., Sharma, M. P., Stock, D. E., 1977. The Particle-Source-In Cell (PSI-CELL) Model for Gas-Droplet Flows. Journal of Fluids Engineering, 325-332.

Estrade, J. P., Carentz, H., Lavergne, G., Biscos, Y., 1999. Experimental in-

vestigation of dynamic binary collision of ethanol droplets - a model for droplet coalescence and bouncing. International Journal of Heat and Fluid Flow 20, 486-491.

Finstad, K. J., Lozowski, E. P., Gates, E. M., 1988. A Computational Investigation of Water Droplet Trajectories. Journal of Atmospheric and Oceanic Technology 5, 160-170.

Gavaises, M., Theodorakakos, A., Bergeles, G., Brenn, G., 1996. Evaluation of the effect of droplet collisions on spray mixing. Proceedings of the Institution of Mechanical Engineers 210, 465-475.

Godard, S., 1960. Mesure de gouttelettes de nuage avec un film de collargol. Bulletin de L'Observatoire du Puy de Dome, 41-46.

Ide, R. F., 1990. Liquid Water Content and Droplet Size Calibration of the NASA Lewis Icing Research Tunnel. NASA TM-102447.

Jeelani, S. A. K., Hartland, S., 1998. Effect of Surface Mobility on Collision of Spherical Drops. Journal of Colloid and Interface Science 206, 83-93.

Karev, A. R., Farzaneh, M., 2002. Evolution of Droplet Size Distribution in an Icing Wind Tunnel. Proceedings of the 10th International Workshop on Atmospheric Icing of Structures.

Karev, A. R., Farzaneh, M., Mousavi, M., 2002. Influence of Non-uniformity of Droplet Size Distribution on Ice Accretion. Proceedings of the 10th International Workshop on Atmospheric Icing of Structures.

Karev, A. R., Farzaneh, M., Lozowski, E. P., 2003. Character and stability of a wind-driven supercooled water film on an icing surface - I. Laminar heat transfer. International Journal of Thermal Sciences 42, 481-498.

Karev, A. R., Farzaneh, M., Lozowski, E. P., 2003. Character and stability of a wind-driven supercooled water film on an icing surface - II. Transition and turbulent heat transfer. International Journal of Thermal Sciences 42,

499-511.

Langmuir, I., Blodgett, K. B., 1945. Mathematical Investigation of Water Droplet Trajectories. Collected works of Irving Langmuir 10, 335-393. Pergamon Press, Oxford.

Lefebvre, A. H., 1989. Atomization and Sprays. Hemisphere Publishing Corporation, New York.

Li, X., 1995. Mechanism of Atomization of a Liquid Jet. Atomization and Sprays 5, 89-105.

Lin, S. P., Reitz, R. D., 1998. Drop and Spray Formation from a Liquid Jet. Annual Review of Fluid Mechanics 30, 85-105.

MacKay, G. D. M., Mason S. G., 1963. The Gravity Approach and Coalescence of Fluid Drops at Liquid Interfaces. The Canadian Journal of Chemical Engineering 41, 203-212.

Makkonen, L., 2000. Models of the growth of rime, glaze, icicles and wet snow on structures. Philosophical Transactions of the Royal Society of London A 358, 2913-2939.

Maxey, M. R., Riley, J. J., 1983. Equation of motion for a small rigid sphere in a nonuniform flow. Physics of Fluids 26(4), 883-889.

Orme, M., 1997. Experiments on Droplet Collisions, Bounce, Coalescence and Disruption. Progression in Energy and Combustion Science 23, 65-79.

O'Rourke, P., Bracco, F., 1980. Modeling of Drop Interactions in Thick Sprays and a Comparison with Experiments. Proceedings of the Institution of Mechanical Engineers 9, 101-116.

Qian, J., Law, C. K., 1997. Regimes of coalescence and separation in droplet collision. Journal of Fluid Mechanics 331, 59-80.

Post, S. L., Abraham, J., 2002. Modeling the outcome of drop-drop collisions in Diesel sprays. International Journal of Multiphase Flow 28, 997-1019.

Reitz, R. D., Bracco, F. V., 1986. Mechanism of Breakup of Round Liquid Jets. The Encyclopedia of Fluid Mechanics, Houston: Gulf Pub. Co., Book Division 3, 233-249.

List of Figures

Figure 11 Vertical distribution of LWC for air stream velocity (a) $u = 5$ m/s (b) $u = 10$ m/s (c) $u = 30$ m/s

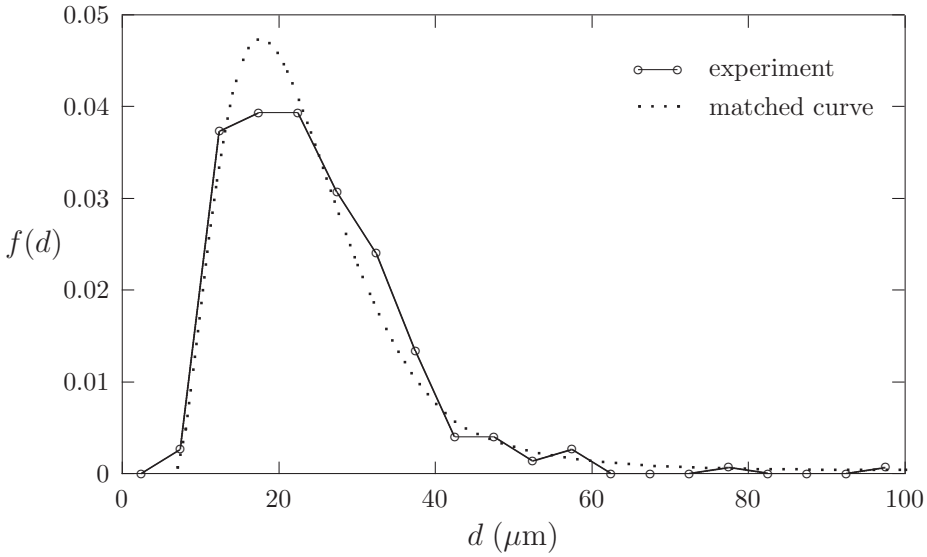
0.05
0.04
0.03
0.02
0.01
0
$f(d)$
0
20
40
60
80
100
d (μm)
experiment
matched curve

Fig. 1.

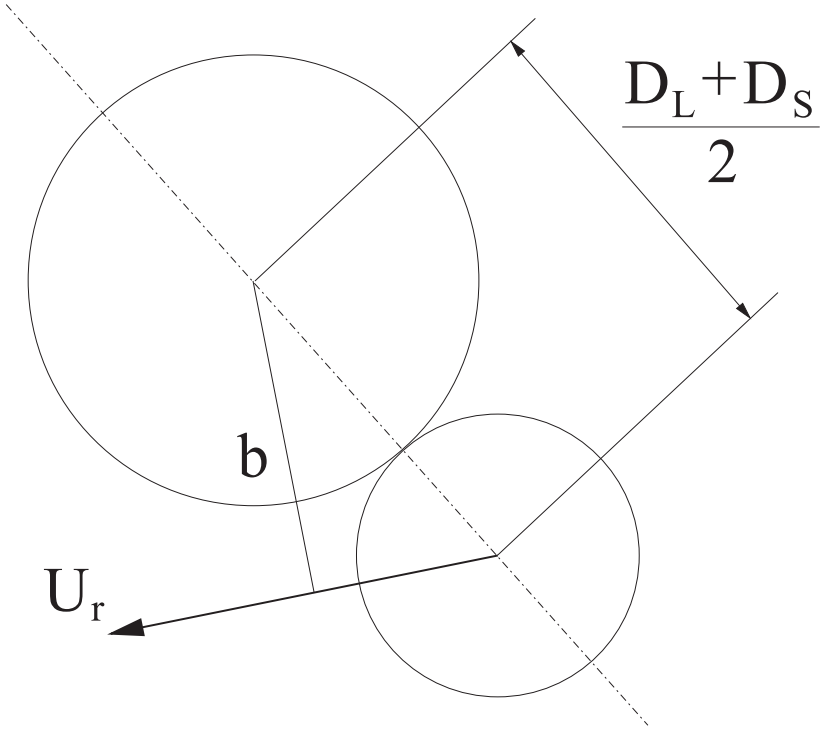
$\frac{D_L+D_S}{2}$
b
U_r

Fig. 2.

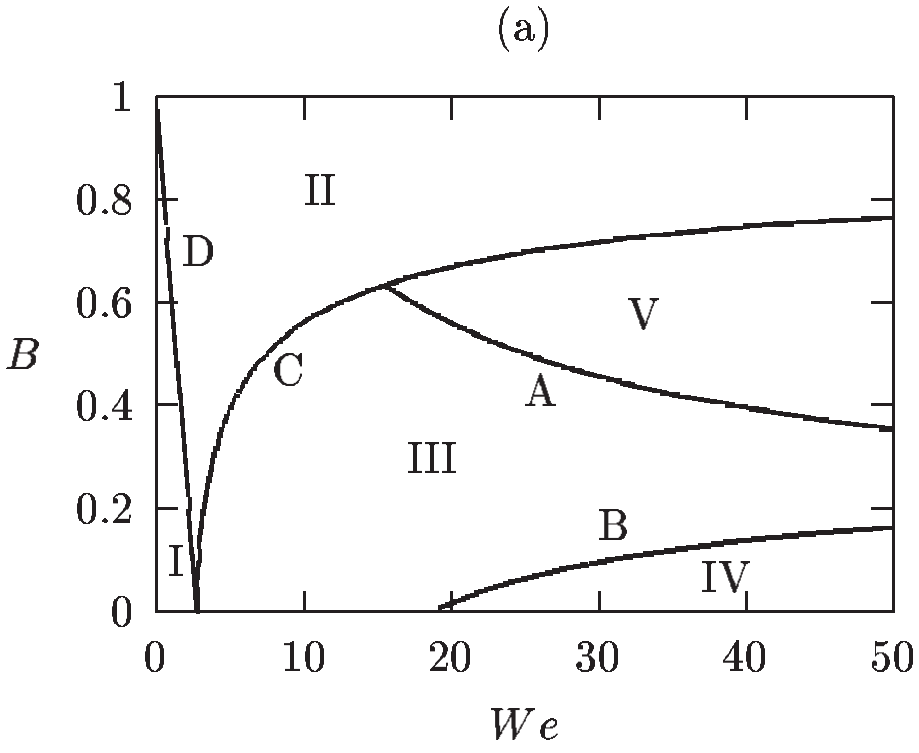
(a)
1
0.8
0.6
0.4
0.2
0
B
0
10
20
30
40
50
We
I
II
III
IV
V
A
B
C
D

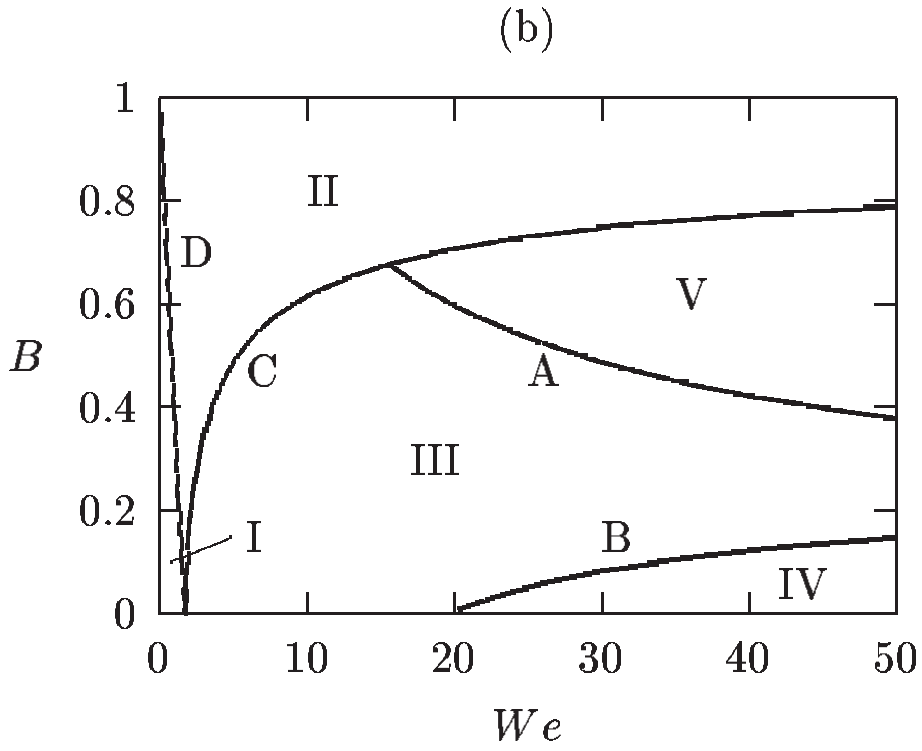
(b)
1
0.8
0.6
0.4
0.2
0
B
0
10
20
30
40
50
We
II
D
V
C
A
III
I
B
IV

(c)

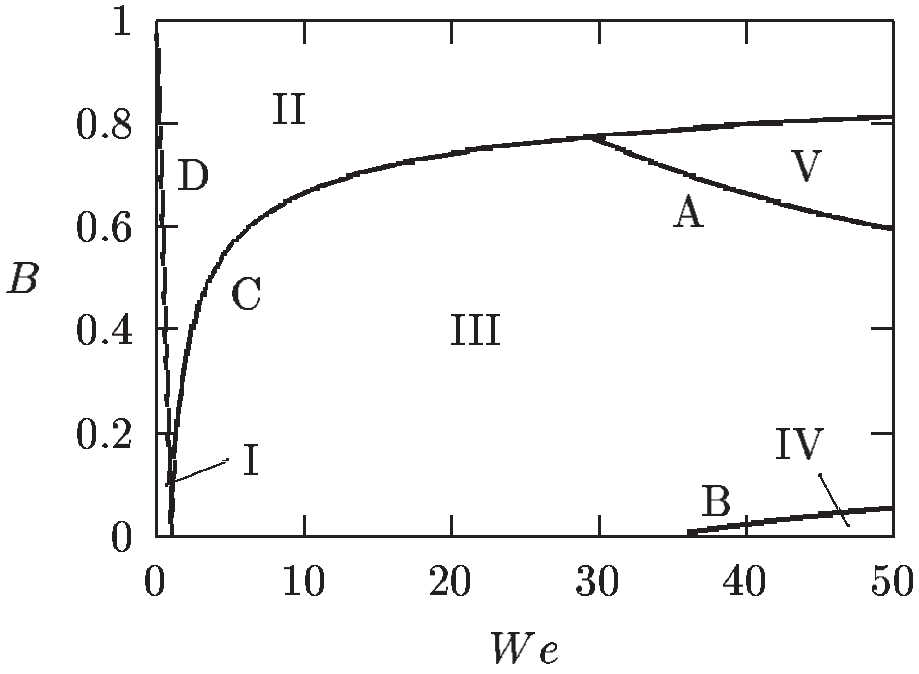
1
0.8
0.6
0.4
0.2
0
B
0
10
20
30
40
50
We
II
D
C
III
I
V
A
IV
B

(d)

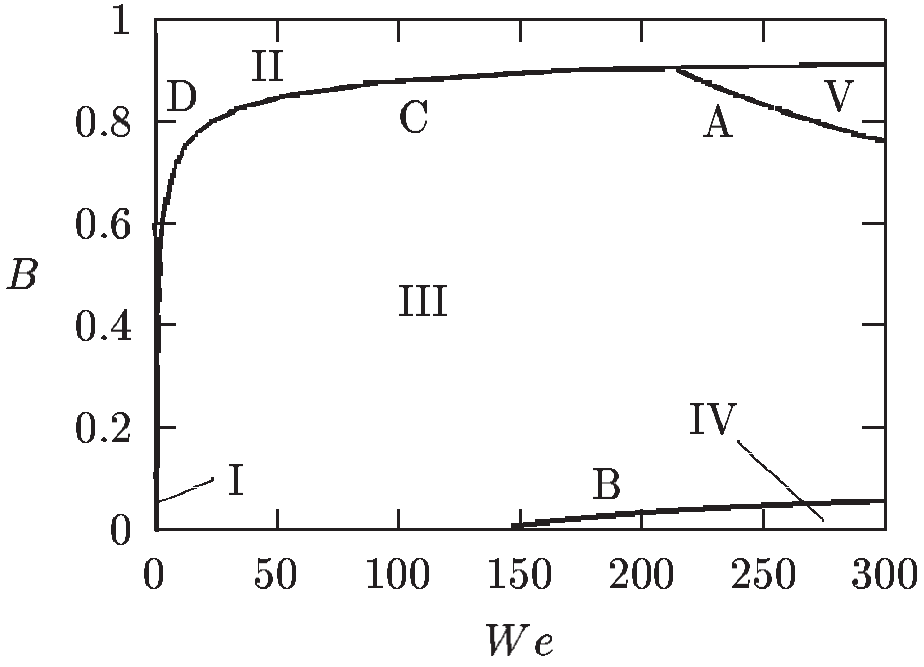
1
0.8
0.6
0.4
0.2
0
B
0
50
100
150
200
250
300
We
II
D
C
III
I
V
A
IV
B

Fig. 3.

(a)

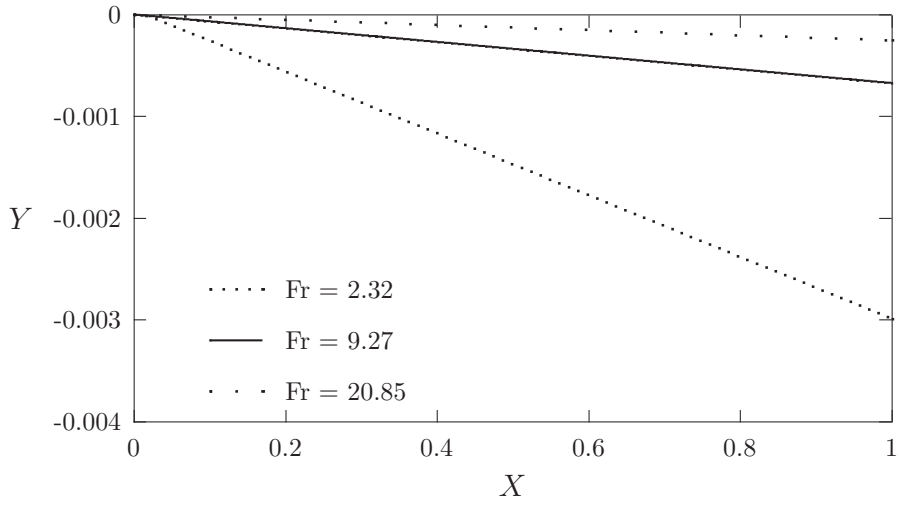
0
-0.001
-0.002
-0.003
-0.004
Y
Fr = 2.32
Fr = 9.27
Fr = 20.85
0
0.2
0.4
0.6
0.8
1
X

(b)

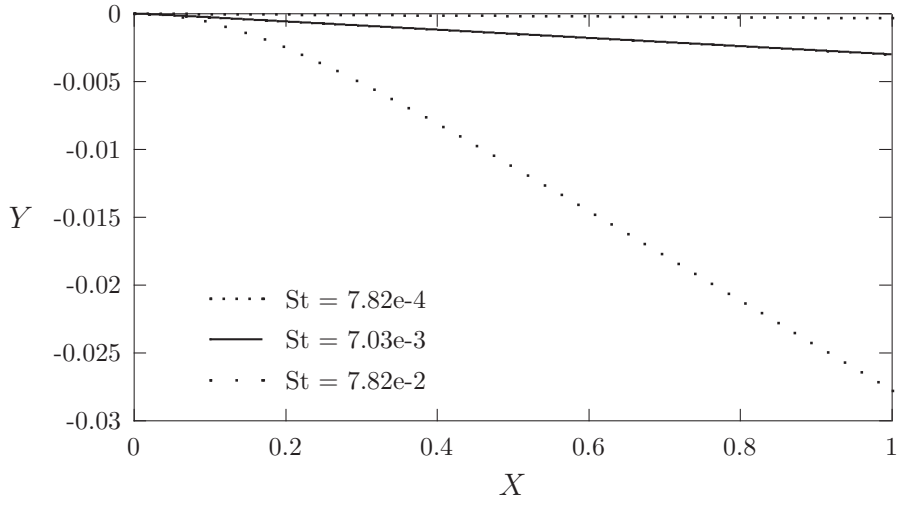
0
-0.005
-0.01
-0.015
-0.02
-0.025
-0.03
Y
St = 7.82e-4
St = 7.03e-3
St = 7.82e-2
0
0.2
0.4
0.6
0.8
1
X

Fig. 4.

(a)

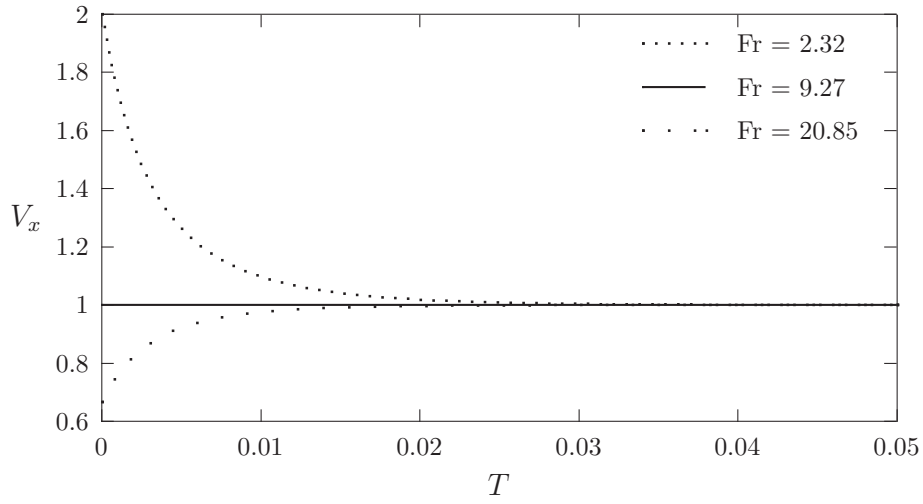

(b)

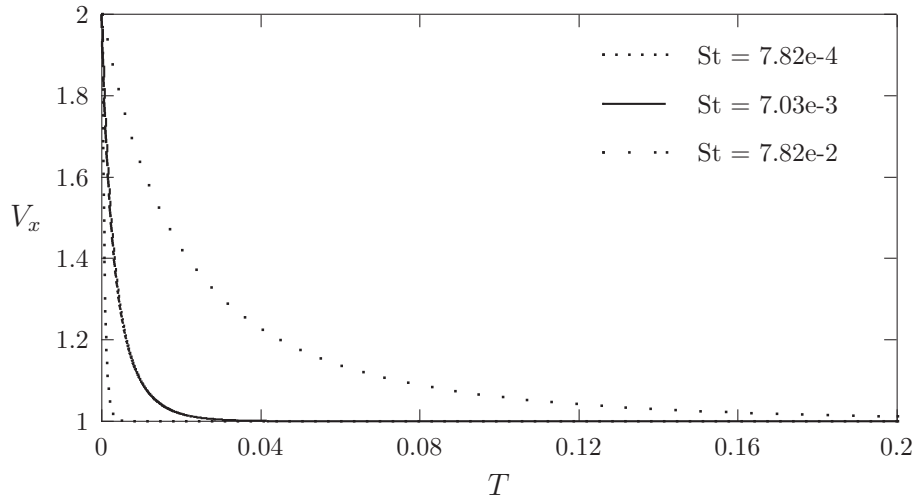

(c)

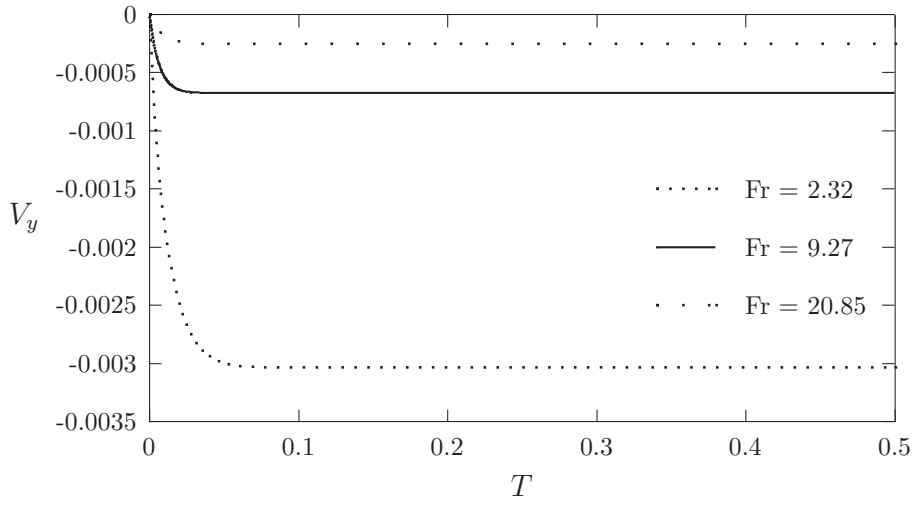
0
-0.0005
-0.001
-0.0015
-0.002
-0.0025
-0.003
-0.0035
V_y
0
0.1
0.2
0.3
0.4
0.5
T
Fr = 2.32
Fr = 9.27
Fr = 20.85

(d)

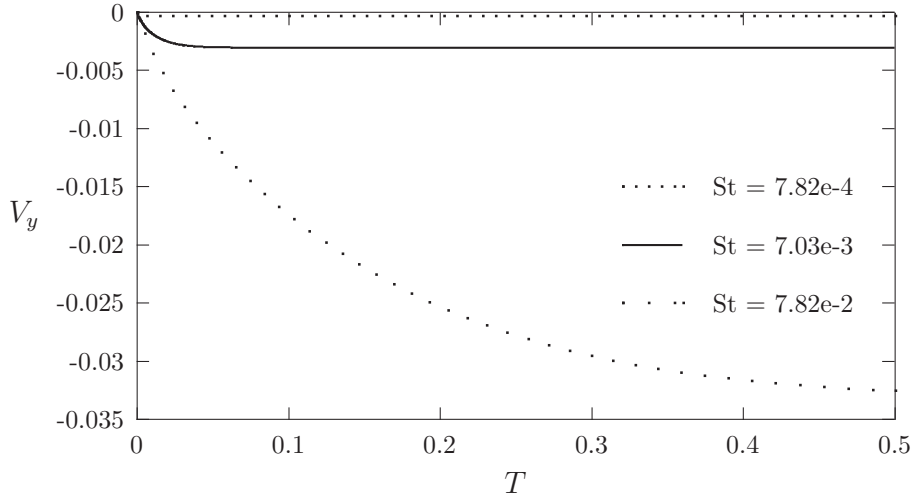
0
-0.005
-0.01
-0.015
-0.02
-0.025
-0.03
-0.035
V_y
0
0.1
0.2
0.3
0.4
0.5
T
St = 7.82e-4
St = 7.03e-3
St = 7.82e-2

Fig. 5.

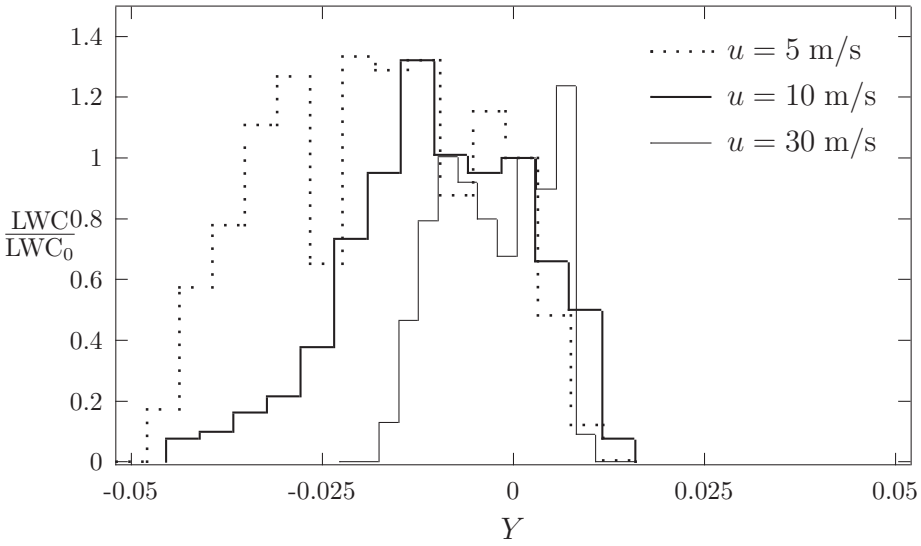
1.4
1.2
1
0.8
0.6
0.4
0.2
0
LWC/LWC0
-0.05
-0.025
0
0.025
0.05
Y
u = 5 m/s
u = 10 m/s
u = 30 m/s

Fig. 6.

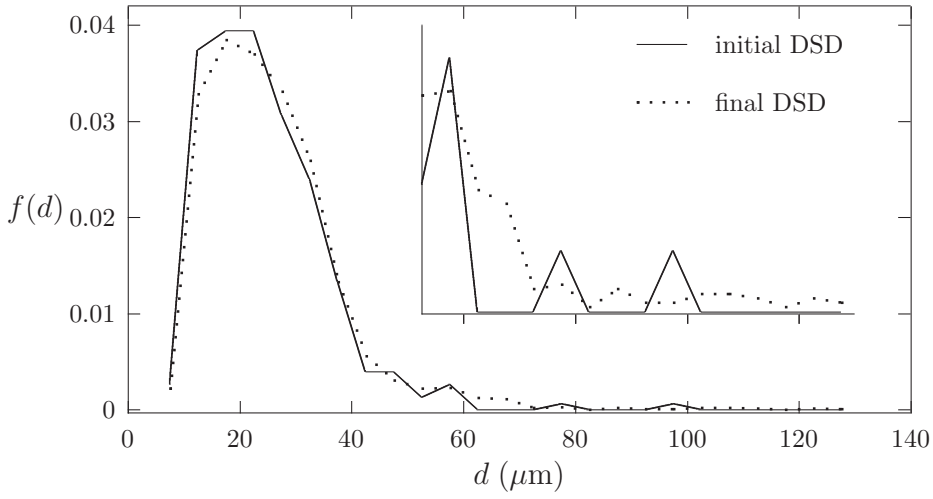
0.04
0.03
0.02
0.01
0
f(d)
0
20
40
60
80
100
120
140
d (μm)
initial DSD
final DSD

Fig. 7.

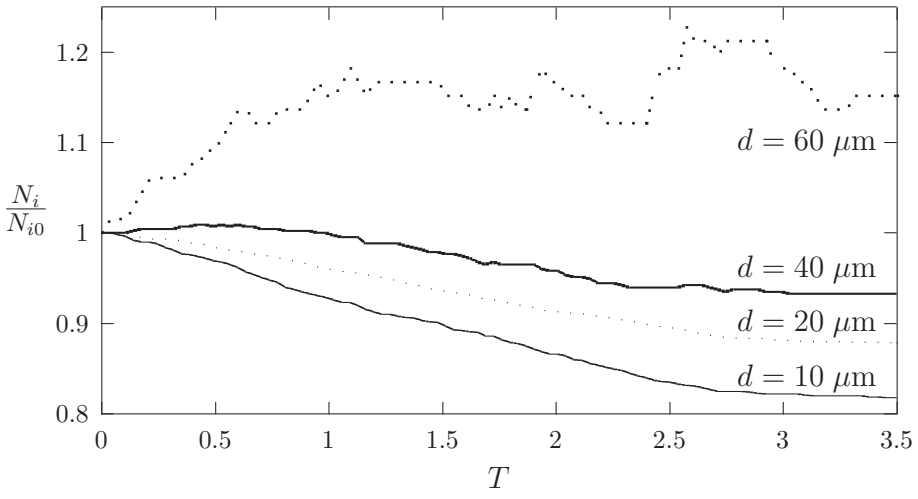
1.2
1.1
1
0.9
0.8
$\frac{N_i}{N_{i0}}$
$d = 60\ \mu\text{m}$
$d = 40\ \mu\text{m}$
$d = 20\ \mu\text{m}$
$d = 10\ \mu\text{m}$
0
0.5
1
1.5
2
2.5
3
3.5
T

Fig. 8.

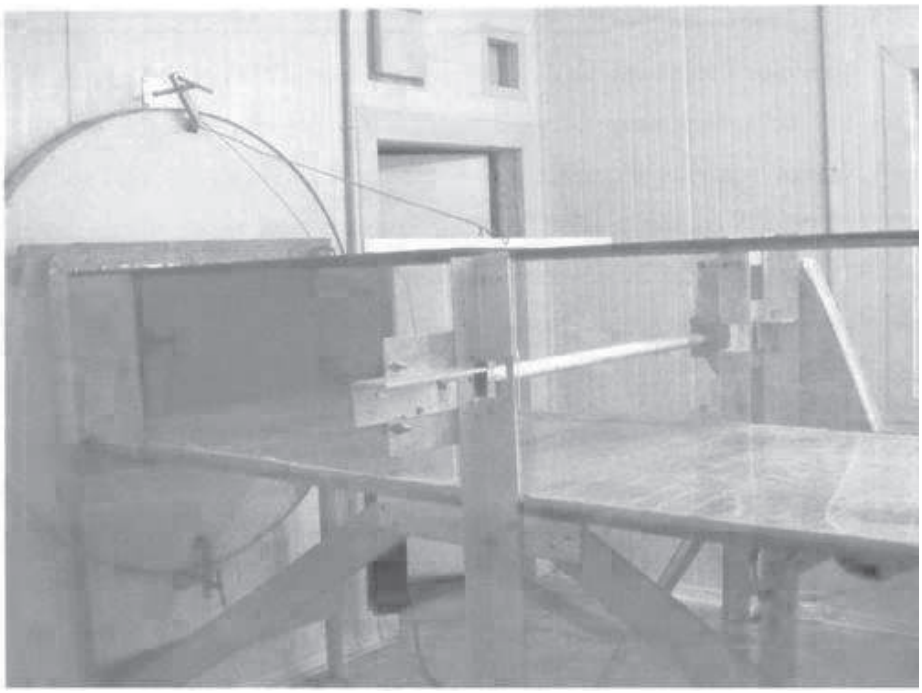

Fig. 9.

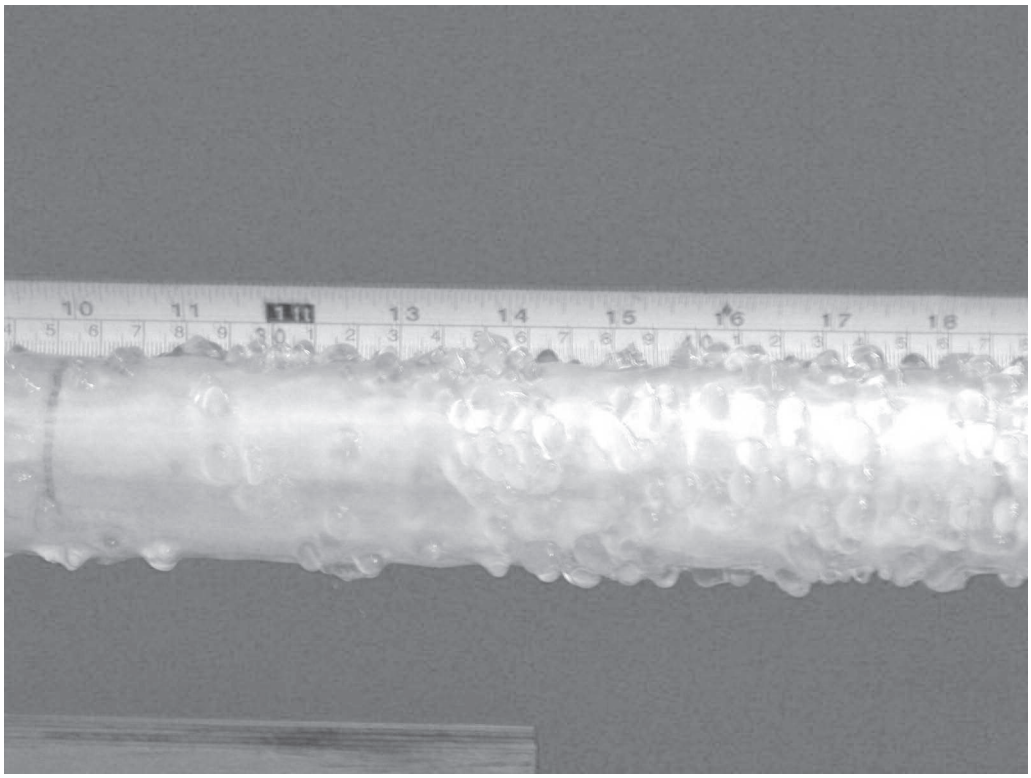

Fig. 10.

(a)

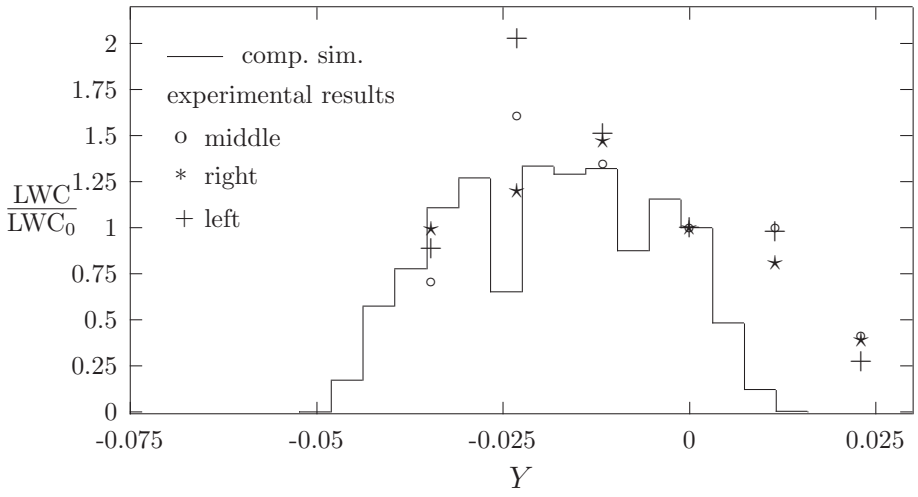
comp. sim.
experimental results
o middle
* right
+ left
LWC/LWC0
Y

(b)

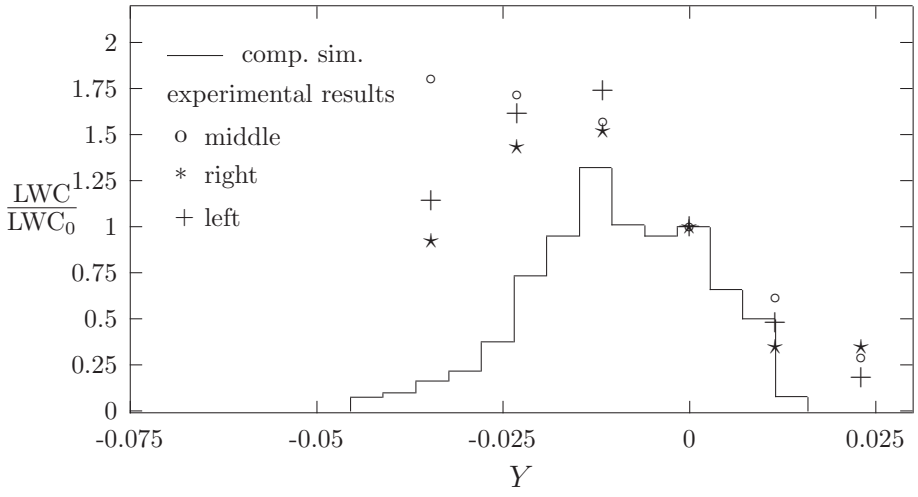
comp. sim.
experimental results
o middle
* right
+ left
LWC/LWC0
Y

(c)

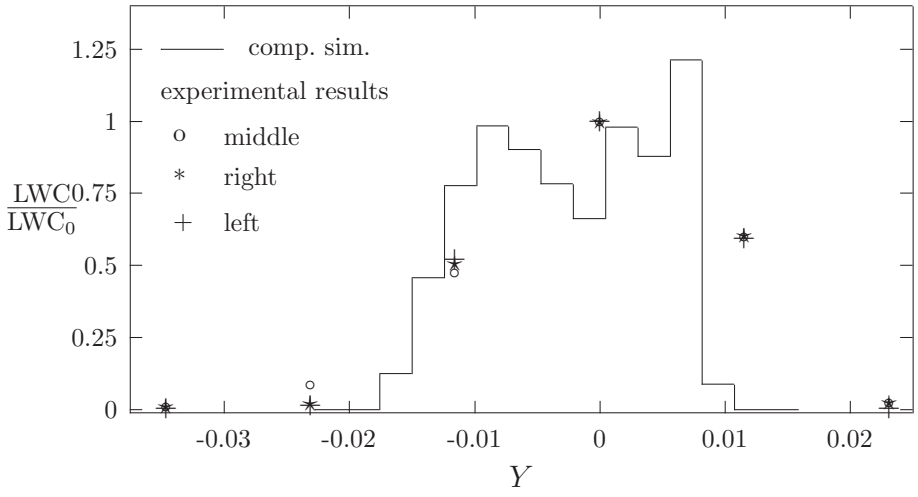
comp. sim.
experimental results
o middle
* right
+ left
LWC/LWC0
Y

Fig. 11.